Optical Fiber Technology 100 (2026) 104650

Contents lists available at ScienceDirect

Optical Fiber Technology

journal homepage: www.elsevier.com/locate/yofte

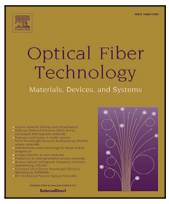

Regular Articles

Tilt-induced anisotropic mode coupling in excessively tilted fiber Bragg gratings for vector bending sensing

Liqing Jing [a,b,c], Kaiming Yang [b,c], Dejun Liu [b,c], Ying Wang [b,c], Yiping Wang [b,c], Chunying Guan [a,*], Changrui Liao [b,*]

[a] Key Laboratory of In-Fiber Integrated Optics of Ministry of Education, College of Physics and Optoelectronic Engineering, Harbin Engineering University, Harbin, 150001, China

[b] State Key Laboratory of Radio Frequency Heterogeneous Integration, Key Laboratory of Optoelectronic Devices and Systems of Ministry of Education/Guangdong Province, College of Physics and Optoelectronic Engineering, Shenzhen University, Shenzhen, 518060, China

[c] Shenzhen Key Laboratory of Ultrafast Laser Micro/Nano Manufacturing, Guangdong and Hong Kong Joint Research Centre for Optical Fibre Sensors, Shenzhen University, Shenzhen, 518060, China

ARTICLE INFO

Keywords:
Excessively tilted fiber Bragg grating
Anisotropic mode coupling
Vector bending sensing
Core–cladding interaction
Femtosecond laser inscription

ABSTRACT

Excessively tilted fiber Bragg gratings (Ex-TFGs) introduce strong transverse refractive-index modulation that significantly modifies the phase-matching conditions between the fundamental core mode and cladding modes. In this work, the tilt-angle-induced anisotropic core-cladding mode coupling in an Ex-TFG is systematically investigated for vector bending sensing. Coupled-mode analysis reveals that the large tilt angle enhances polarization-dependent interaction and produces asymmetric modal overlap under transverse bending perturbations. This anisotropic coupling leads to direction-dependent attenuation of selected cladding modes, resulting in a characteristic figure-eight angular response. The physical origin of this behavior is attributed to tilt-enhanced redistribution of strain-induced effective-index variation along the grating planes. Experimental results demonstrate a maximum bending sensitivity of 0.16 dB m^{-1}, with sensitivity maxima at 0° and 180° and minima at 90° and 270°. The results clarify the mechanism of tilt-controlled anisotropic mode coupling and establish Ex-TFGs as an effective platform for direction-resolved fiber-optic sensing.

1. Introduction

Understanding strain-induced modal interaction under transverse bending is fundamental to direction-resolved fiber sensing. Conventional fiber Bragg gratings (FBGs) have been widely employed for axial strain sensing owing to their compact structure and wavelength-encoded response. However, their intrinsic longitudinal symmetry and reliance on axial strain-induced Bragg wavelength shifts limit their capability in resolving multidirectional bending and transverse perturbations, often requiring multiple sensing elements or high-resolution spectral interrogation systems [1,2].

Tilted fiber Bragg gratings (TFBGs), formed by inclining the grating planes with respect to the fiber axis, break the longitudinal symmetry of standard FBGs and enable phase-matched coupling between the fundamental core mode and a series of cladding modes [3–5]. The tilt-angle-dependent coupling coefficient enhances sensitivity to transverse perturbations such as bending and torsion. In particular, excessively tilted fiber Bragg gratings (Ex-TFGs), characterized by large tilt angles, further strengthen core–cladding mode interaction and introduce pronounced anisotropic modal behavior [6–8]. The large tilt angle significantly alters the phase-matching condition and redistributes the modal overlap integral between orthogonal cladding modes and external perturbations, enabling polarization-dependent and direction-resolved sensing characteristics [9–11]. Various alternative bending sensing configurations, including interferometric structures, long-period gratings, and microbend-based devices, have also been reported [12–15]. While these approaches offer distinct advantages, they often involve complex fabrication processes or limited control over directional selectivity.

In this work, we investigate the anisotropic core–cladding mode coupling in an excessively tilted fiber Bragg grating and demonstrate an intensity-modulated bending sensing scheme based on a single-grating configuration. By exploiting tilt-induced asymmetric modal redistribution under transverse bending, the proposed structure enables simultaneous measurement of bending magnitude and direction. Experimental results confirm a maximum bending sensitivity of 0.16 dB m^{-1} and a pronounced figure-eight angular response, thereby clarifying the physical origin of tilt-induced anisotropic mode coupling.

* Corresponding authors.
E-mail addresses: cyguan@163.com (C. Guan), cliao@szu.edu.cn (C. Liao).

https://doi.org/10.1016/j.yofte.2026.104650
Received 15 February 2026; Received in revised form 28 March 2026; Accepted 3 April 2026
Available online 20 April 2026
1068-5200/© 2026 Elsevier Inc. All rights are reserved, including those for text and data mining, AI training, and similar technologies.

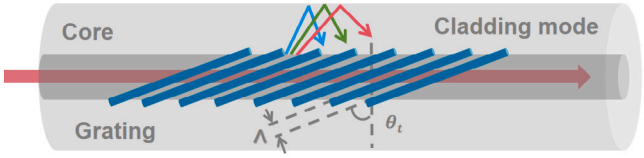

Fig. 1. Schematic structure of Ex-TFG.

2. Principles

Excessively tilted fiber Bragg gratings (Ex-TFGs) enable efficient coupling between the fundamental core mode and multiple cladding modes due to their large tilt angle. As schematically illustrated in Fig. 1, the tilted grating planes introduce both axial and transverse components of the refractive-index modulation vector. Similar to long-period gratings (LPGs) in terms of cladding-mode excitation, the excessive tilt in Ex-TFGs breaks the cylindrical symmetry of the fiber and results in asymmetric refractive-index modulation [16,17]. The axial projection of the grating vector governs the phase-matching condition, while the transverse component enhances the core–cladding interaction. Consequently, multiple cladding modes can be excited, resulting in characteristic resonance features in the transmission spectrum. Furthermore, through polarization control, orthogonal cladding-mode polarizations (fast and slow axes) can be selectively addressed, providing the physical basis for directional bending sensitivity [18].

According to coupled-mode theory, the interaction between the core mode and a dominant mth cladding mode can be expressed as [19]:

$$\frac{dA_{\text{core}}}{dz} = -j\kappa_m A_{\text{clad},m} e^{-j\Delta\beta_m z}, \tag{1}$$

$$\frac{dA_{\text{clad},m}}{dz} = -j\kappa_m A_{\text{core}} e^{+j\Delta\beta_m z}, \tag{2}$$

where A_{core} and $A_{\text{clad},m}$ represent the amplitudes of core and cladding modes respectively, κ_m is the coupling coefficient, dependent on the grating tilt angle, period, and refractive index profile, and $\Delta\beta_m = \beta_{\text{core}} - \beta_{\text{clad},m}$ is the propagation constant mismatch between core and cladding modes. z is the propagation distance along the fiber.

The phase matching condition essential for efficient mode coupling is given by [20]:

$$\Delta\beta_m = \beta_{\text{core}} - \beta_{\text{clad},m} = \frac{2\pi}{\Lambda}\cos(\theta_t). \tag{3}$$

where Λ is the grating period and θ_t is the tilt angle defined as the angle between the grating planes and the plane perpendicular to the fiber axis. The propagation constant β is defined in terms of the effective refractive index (n_{eff}).

$$\beta = \frac{2\pi n_{\text{eff}}}{\lambda}. \tag{4}$$

Substituting Eq. (3) into Eq. (2), we explicitly define mode coupling conditions related to refractive index changes:

$$\frac{2\pi}{\lambda}\left(n_{\text{core}} - n_{\text{clad},m}\right) = \frac{2\pi}{\Lambda}\cos(\theta_t). \tag{5}$$

When the fiber undergoes bending with radius R, the axial strain ε_z at a radial position r in the fiber is given by:

$$\varepsilon_z(r) = \frac{r}{R}. \tag{6}$$

where r is the radial position within the fiber, and R is the bending radius. However, the transverse strain ε_t is the strain that influences refractive index modulation due to the strain-optic effect. It is related to axial strain by Poisson's ratio ν:

$$\varepsilon_t = -\nu\varepsilon_z = -\nu\frac{r}{R}. \tag{7}$$

where ν is the Poisson's ratio of the fiber material, ε_z is the axial strain. The strain-optic effect links refractive index change Δn to the transverse strain ε_t.

$$\Delta n = -\frac{1}{2}n_0^3(p_{11} - p_{12})\,\varepsilon_t. \tag{8}$$

where n_0 is the original refractive index of the fiber core material, p_{11} and p_{12} are the strain-optic coefficients of the fiber material.

By substituting Eq. (7) into Eq. (8), we obtain a direct link between bending curvature and refractive index variation:

$$\Delta n = -\frac{1}{2}n_0^3(p_{11} - p_{12})\,\nu\,\frac{r}{R}. \tag{9}$$

These refractive-index variations perturb β_{core} and $\beta_{\text{clad},m}$, modifying the phase-matching condition and mode-coupling efficiency. Under bending, the refractive-index distribution becomes asymmetric, introducing a curvature dependence on the effective attenuation coefficient.

The curvature magnitude is defined as $\kappa = 1/R$, where R is the bending radius. The bending-induced intensity variation follows an exponential attenuation law:

$$I(\kappa,\varphi) = I_0\exp[-\alpha(\kappa,\varphi)L], \tag{10}$$

where I_0 is the input reference intensity and L is the grating length. The bending direction φ is defined as the azimuth angle measured from the plane of the tilted grating, corresponding to the high-sensitivity axis of the Ex-TFG.

For small curvatures, the excess attenuation is linearized with respect to κ and decomposed into isotropic and anisotropic components as

$$\alpha(\kappa,\varphi) = \alpha_0 + \kappa(\alpha_{\text{iso}} + \alpha_{\text{an}}\cos 2\varphi), \tag{11}$$

where α_0 is the baseline attenuation, α_{iso} characterizes the isotropic bending-induced loss, and α_{an} captures the anisotropic term originating from the tilt-induced asymmetric refractive-index perturbation and polarization-dependent core–cladding coupling.

Substituting Eq. (11) into Eq. (10) yields

$$I(\kappa,\varphi) = I_0\exp\{-L[\alpha_0 + (\alpha_{\text{iso}} + \alpha_{\text{an}}\cos 2\varphi)\kappa]\}. \tag{12}$$

Differentiating Eq. (12) with respect to κ and normalizing by the transmitted intensity yields the logarithmic curvature sensitivity:

$$S(\varphi) = \frac{\partial \ln I}{\partial\kappa} = \frac{1}{I}\frac{\partial I}{\partial\kappa} = -L(\alpha_{\text{iso}} + \alpha_{\text{an}}\cos 2\varphi). \tag{13}$$

The isotropic term contributes only to a curvature-independent offset and does not affect the angular dependence. Therefore, the purely directional component of the sensitivity can be expressed as

$$S(\varphi) = S_{\max}\cos 2\varphi, \qquad S_{\max} = L\alpha_{\text{an}}. \tag{14}$$

It should be emphasized that the above formulation captures the dominant anisotropic coupling mechanism rather than providing a full modal-resolved quantitative model. In excessively tilted fiber Bragg gratings, higher-order cladding modes exhibit stronger evanescent-field interaction and enhanced sensitivity to transverse perturbations. The experimentally selected resonance corresponds to a strong and stable cladding-mode feature, enabling reliable tracking of bending-induced intensity variation. Although multiple cladding modes coexist, their angular responses are governed by the same tilt-induced anisotropic coupling mechanism. Therefore, the observed figure-eight response represents a general system characteristic rather than a feature of a specific mode order. The agreement between the experimental results and the predicted $\cos(2\varphi)$ dependence confirms that tilt-induced anisotropic core–cladding mode coupling dominates the sensing mechanism.

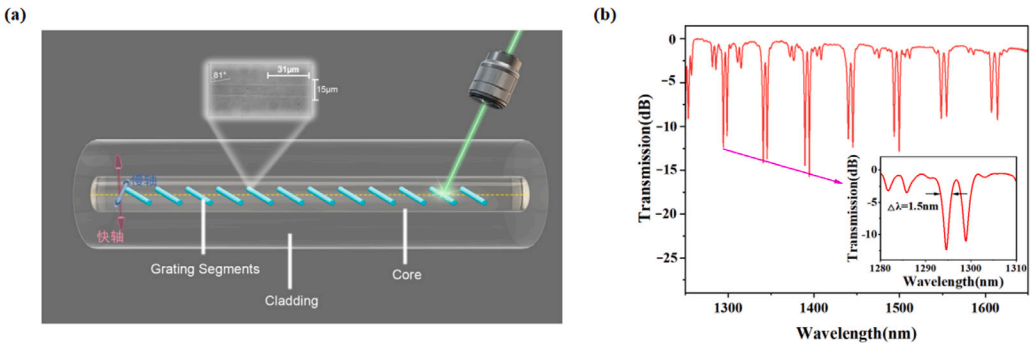

Fig. 2. (a) Schematic diagram of the Ex-TFG fabrication setup. Inset: Optical microscope image of the fabricated Ex-TFG structure. (b) Transmission spectrum of the fabricated Ex-TFG. Inset: Enlarged view of the dual-resonance features.

3. Sensors design and fabrication

The performance of Ex-TFGs is closely related to the grating tilt angle, which requires precise fabrication control to ensure stable mode coupling characteristics. Femtosecond laser direct writing provides a flexible and accurate method for fabricating Ex-TFGs, offering high spatial resolution and compatibility with various fiber types [21,22]. Compared with UV inscription and phase-mask techniques, the nonlinear absorption–based femtosecond laser process allows direct inscription of large tilt angles (>80°) with localized refractive-index modification and sub-micrometer positioning accuracy. During fabrication, the fiber was mounted on an air-bearing translation stage (Aerotech) to ensure stable motion control. A femtosecond laser (λ = 515 nm, pulse duration ≈290 fs, repetition rate = 100 kHz) with an average power of 1.14 mW (11.4 nJ per pulse) was focused into the fiber core using a 100× oil-immersion objective (NA = 1.32) after removal of the polymer coating. The fabricated Ex-TFGs exhibited clear and uniform grating structures, as shown in Fig. 2(a). The grating was inscribed using a line-by-line femtosecond laser scanning method. This method ensures well-defined grating plane orientation and consistent refractive index modulation, which is essential for achieving stable anisotropic coupling behavior. Specifically, the focused laser beam was scanned transversely across the fiber core to form individual refractive index modification tracks, while the fiber was simultaneously translated along its axis to construct the tilted grating planes. This inscription strategy enables precise control of the tilt angle and refractive index modulation profile, and is widely used for fabricating excessively tilted fiber Bragg gratings.

The grating period was 31 μm, and the grating planes were tilted by 81° with respect to the plane perpendicular to the fiber axis. The transmission spectrum in Fig. 2(b) shows distinct dual-peak resonances corresponding to two orthogonal cladding-mode families (fast and slow axes). Each resonance exhibits a linewidth of approximately (~0.4 nm) and a modulation depth of ~16 dB. The consistency and repeatability of the femtosecond laser direct-writing process demonstrate its suitability for fabricating Ex-TFG sensors for intensity-based bending measurement.

4. Results and discussion

4.1. Vector bending response characterization

The vector bending response of the fabricated Ex-TFG sensor was experimentally characterized using the setup illustrated in Fig. 3(a). The sensor was mounted between two rotational fiber clamps (Newport model 466A-718) fixed on high-precision three-dimensional translation stages, allowing controlled adjustment of bending curvature and direction. The bending curvature was varied by changing the clamp separation, while the bending direction was adjusted by rotating both clamps simultaneously. This configuration ensures pure bending without introducing torsion, enabling independent control of bending magnitude and azimuth angle. It should be noted that the influence of light source power fluctuation and polarization instability is minimized by using a stable broadband source and fixed polarization conditions. Residual fluctuations have negligible impact on the observed angular response. The angular response of the selected resonance was experimentally evaluated as a function of bending direction. As illustrated in Fig. 3(b), the bending direction angle φ is defined as the angle between the fiber's bending plane and the slow axis of the Ex-TFG.

When $\varphi = 0°$ and 180°, the bending direction aligns with the high-sensitivity axis, resulting in maximum intensity variation. In contrast, when φ = 90° and 270°, the response is minimized. This angular dependence is consistent with the theoretical prediction described in Section 2, confirming that bending-induced intensity variation originates from anisotropic core–cladding mode coupling.

The sensor response was first evaluated by varying the bending curvature from 4.4 m^{-1} to 20.0 m^{-1} while keeping the bending direction fixed. As shown in Fig. 4(a), several cladding-mode resonances (peaks 2–5) exhibit curvature-dependent intensity modulation. Peaks 2 and 3 show nearly identical variation trends, whereas peaks 4 and 5 follow a distinct but internally consistent response pattern, as illustrated in Fig. 4(b). Peaks 2 and 3 arise from nearly degenerate orthogonally polarized cladding modes belonging to the same modal family, leading to similar effective indices and comparable modal confinement. Consequently, they exhibit nearly identical intensity–curvature characteristics, suggesting that their bending response is primarily governed by polarization degeneracy. In contrast, peaks 4 and 5 correspond to higher-order cladding modes with more extended field distributions, which experience stronger bending-induced radiation loss and therefore display distinct curvature dependence. Among the observed resonances, peak 3 demonstrates stable spectral characteristics and monotonic intensity response over the investigated curvature range, and is therefore selected as the representative resonance for subsequent vector-bending characterization. This selection also minimizes the influence of spectral noise and mode overlap from adjacent resonances, thereby improving the reliability of the extracted bending response. In addition to the dominant resonances, several weaker spectral features can be observed, which are attributed to coupling to adjacent cladding modes with lower coupling efficiency. Due to their relatively low signal-to-noise ratio and limited contribution to sensing performance, these modes are not considered in the quantitative analysis.

Subsequently, the bending curvature was fixed at 20 m^{-1}, and the bending direction angle φ was varied from 0° to 360° in 30° increments. The directional response of peak 3 was characterized in terms of its resonance wavelength shift, as shown in Fig. 5(a) and Fig. 5(b). A redshift is observed as φ increases from 0° to 180°, while a corresponding blueshift occurs from 180° to 360°. This symmetric wavelength variation reflects the anisotropic strain redistribution along the tilted grating planes under transverse bending. It is worth noting that the wavelength shift is relatively small compared with the intensity variation. This is because the proposed sensor operates

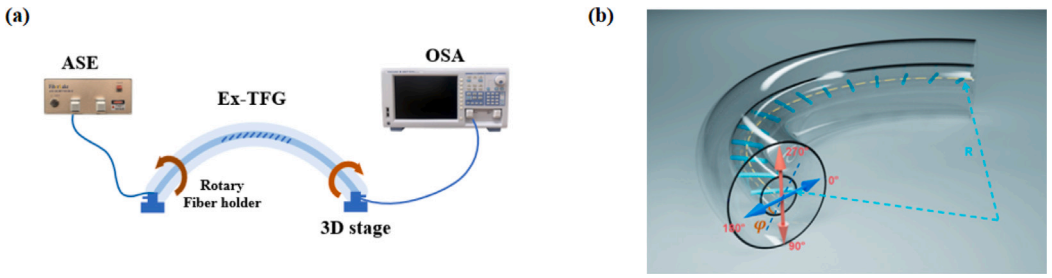

Fig. 3. (a) Schematic diagram of the experimental setup for vector bending measurement using the Ex-TFG sensor. (b) Definition of the bending direction angle φ.

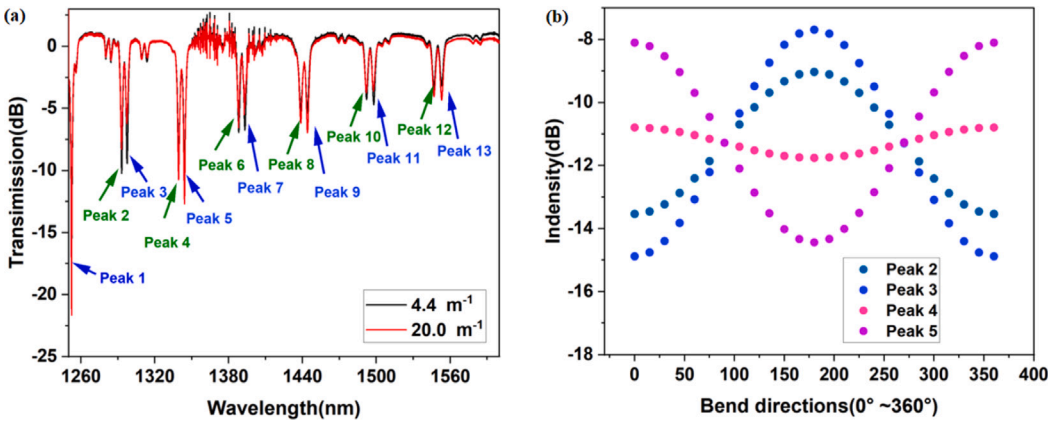

Fig. 4. Transmission spectra of the Ex-TFG sensor under two different bending curvatures: 4.4 m^{-1} and 20.0 m^{-1}, with a fixed bending direction. (b) Intensity variations of peaks 2, 3, 4, and 5 as a function of bending direction at a fixed curvature of 20.0 m^{-1}.

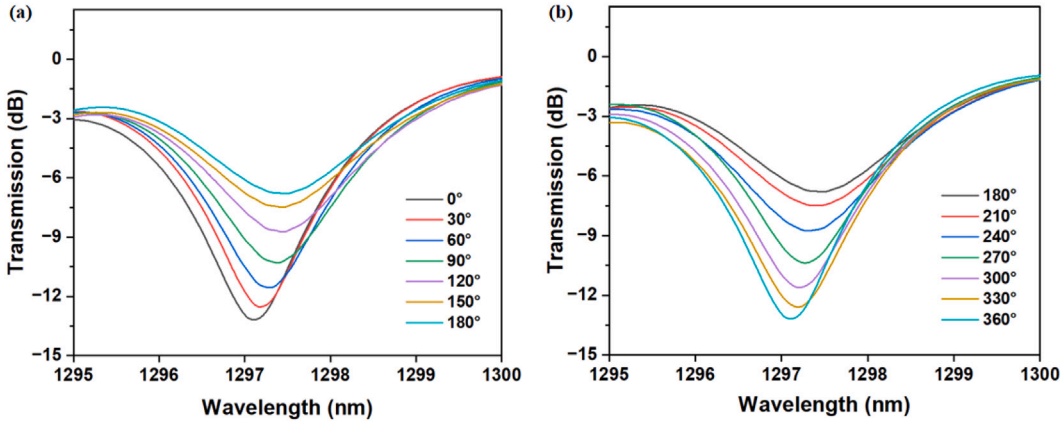

Fig. 5. Resonance wavelength shift of Peak 3 under varying bending direction angles (φ). (a) Redshift observed as φ increases from 0° to 180°, due to increasing tensile strain. (b) Blueshift observed as φ increases from 180° to 360°, due to transition to compressive strain.

primarily through intensity modulation, with the bending information encoded in the anisotropic attenuation of the cladding modes rather than in wavelength tracking. Therefore, the modest wavelength shift does not limit the functionality of the proposed vector bending sensing scheme. The bending sensitivity was further quantified by monitoring the resonance intensity of peak 3 while sweeping the bending direction from 0° to 360° in 15° increments at multiple curvatures between 4.4 and 20.0 m^{-1}. The directional sensitivity, defined as the change in resonance intensity between the two curvature states, exhibits a pronounced angular dependence. The extracted sensitivities plotted in polar coordinates (Fig. 6(b)) reveal a clear figure-eight pattern, with maxima at $\varphi = 0°$ and 180° and minima near 90° and 270°.

This angular behavior agrees well with the $\cos(2\varphi)$ dependence predicted by Eq. (14), confirming that the second-order harmonic arises from the anisotropic attenuation coefficient $\alpha(K, \varphi)$. Minor deviations from the ideal $\cos(2\varphi)$ profile can be attributed to fabrication asymmetry, polarization misalignment, and higher-order bending effects not captured in the first-order model. The sign of the extracted sensitivity reflects the relative dominance between coupling-strength enhancement and bending-induced radiation attenuation. For orientations aligned with the high-sensitivity axis, the asymmetric redistribution of modal overlap enhances core–cladding coupling, resulting in increased resonance intensity. Conversely, when bending aligns with the

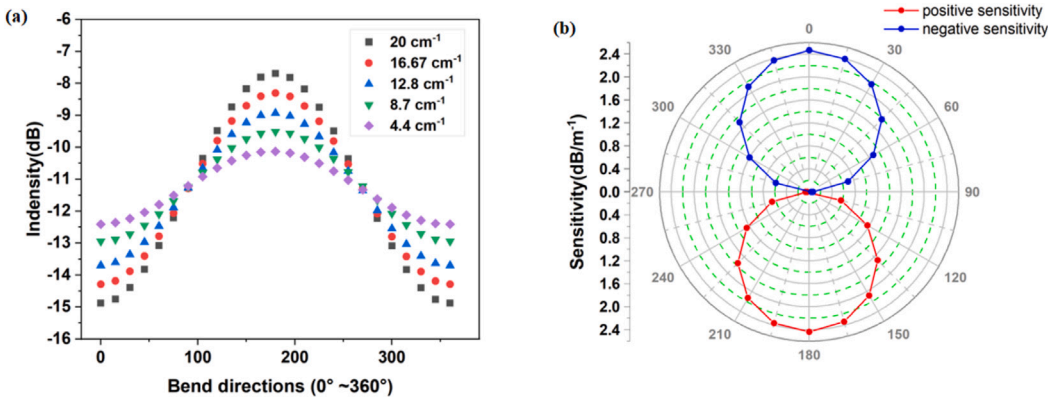

Fig. 6. (a) Resonance intensity response of the Ex-TFG sensor under varying bending curvatures and directions. (b) Bending sensitivity plotted in polar coordinates as a function of bending direction angle (φ, 0°–360°).

Table 1
Comparison of representative two-dimensional vector bending fiber-optic sensors.

Sensor type	Principle	Sensitivity type	Max sensitivity	Speed	Directionality	Complexity
Proposed Ex-TFG	Intensity	dB m^{-1}	0.16	Fast	High	Low (simple & cost-effective)
Multicore FBG [23]	Wavelength	pm m^{-1}	59.47	Slower (Requires spectral analysis)	High	Moderate
Orthogonal cladding-type helical FBGs [24]	Wavelength	pm m^{-1}	50	Slower (Requires spectral analysis)	High	High (complex structure & high cost)
Edge-core FBG [25]	Hybrid	dB m^{-1} & pm m^{-1}	0.22/59.7	High	High	Moderate
LPG [14]	Wavelength	nm m^{-1}	8.53	Slower (Requires spectral analysis)	Low	High (complex structure)

orthogonal axis, radiation leakage of the excited cladding modes dominates, leading to reduced resonance depth and negative sensitivity.

Finally, the resonance intensity as a function of bending curvature was analyzed for selected bending directions, as shown in Fig. 7. A nearly linear dependence is observed over the investigated curvature range, confirming the stability of the intensity-modulated detection scheme. The maximum measured bending sensitivity reaches approximately −0.16 dB m^{-1}. Based on the ratio between the system noise level and the measured sensitivity, the curvature resolution is estimated to be on the order of 0.1 m^{-1}.

The clear directional dependence and symmetric figure-eight angular profile validate the anisotropic attenuation model introduced in Section 2. The agreement between experimental data and the predicted $\cos(2\phi)$ behavior indicates that the dominant sensing mechanism originates from tilt-induced anisotropic core–cladding mode coupling.

4.2. Comparative analysis of fiber-optic bending sensors

Table 1 presents a comparison of representative two-dimensional vector bending fiber-optic sensors reported in the literature, focusing on measurement principle, sensitivity type, maximum sensitivity, response speed, directional capability, and system complexity. Conventional wavelength-shift-based configurations, including multicore FBGs [23], orthogonal cladding-type helical FBGs [24], edge-core cladding FBGs [25], and long-period gratings (LPGs) [14], generally achieve high wavelength sensitivities (ranging from tens of pm m^{-1} to several nm m^{-1}). However, these approaches typically rely on spectral interrogation and often require multi-element structures or polarization-resolved detection schemes, resulting in increased system complexity and slower response speed. In contrast, the proposed Ex-TFG sensor operates under an intensity-modulated mechanism with a maximum bending sensitivity of 0.16 dB m^{-1}. Although the sensitivity is moderate compared with wavelength-based configurations, the proposed Ex-TFG sensor offers several distinct advantages. First, the intensity-modulated mechanism eliminates the need for spectral tracking, enabling faster response and simpler interrogation systems. Second, the single-grating configuration significantly reduces fabrication complexity compared with multicore or hybrid structures. More importantly, the proposed sensor intrinsically provides directional discrimination without requiring multiple sensing elements or polarization-resolved detection. This represents a practical trade-off between sensitivity and system simplicity, making the proposed design particularly suitable for real-time and cost-effective applications.

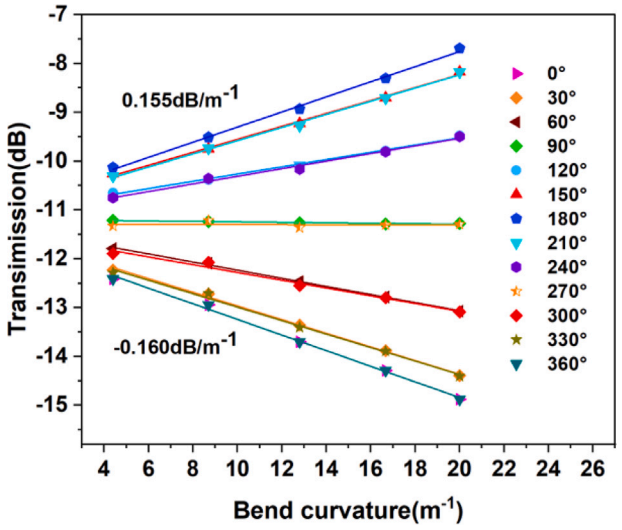

Fig. 7. The relationship between resonance intensity and bending curvature at various bending directions.

5. Conclusion

In this work, an excessively tilted fiber Bragg grating (Ex-TFG) sensor for vector bending measurement was proposed and experimentally demonstrated based on an intensity-modulated detection scheme. Owing to the large grating tilt angle, enhanced anisotropic core–cladding mode coupling enables direction-resolved bending sensing within a single-grating configuration. The sensor exhibits a maximum bending sensitivity of 0.16 $\mathrm{dB\,m^{-1}}$ and a pronounced figure-eight angular dependence, with sensitivity maxima at $\varphi = 0°$ and 180°, and minima at $\varphi = 90°$ and 270°. The experimental observations agree well with the theoretically predicted $\cos(2\varphi)$ behavior derived from tilt-induced anisotropic attenuation. The proposed Ex-TFG structure provides a compact and robust platform for direction-resolved fiber-optic sensing and offers a practical approach for vector bending monitoring in structural health and advanced optical sensing applications. Future work will focus on improving sensitivity through structural optimization and developing a more comprehensive modal analysis framework.

CRediT authorship contribution statement

Liqing Jing: Writing – review & editing, Writing – original draft, Investigation, Formal analysis, Data curation, Conceptualization. **Kaiming Yang:** Visualization, Formal analysis. **Dejun Liu:** Software, Resources. **Ying Wang:** Validation, Software. **Yiping Wang:** Investigation. **Chunying Guan:** Validation, Data curation, Conceptualization. **Changrui Liao:** Resources, Investigation, Data curation.

Declaration of competing interest

The authors declare that they have no known competing financial interests or personal relationships that could have appeared to influence the work reported in this paper.

Acknowledgments

This work was supported by the National Key Research and Development Program of China (2024YFB3213700) and the National Natural Science Foundation of China (T2421003, U22A2088).

Data availability

Data will be made available on request.

References

[1] Q. Wang, Y. Liu, Review of optical fiber bending/curvature sensor, Measurement 130 (2018) 161–176.
[2] C.C. Ye, S.W. James, R.P. Tatam, Simultaneous temperature and bend sensing with long-period fiber gratings, Opt. Lett. 25 (14) (2000) 1007–1009.
[3] X. Dong, H. Zhang, B. Liu, Y. Miao, Tilted fiber Bragg gratings: Principle and sensing applications, Photonic Sensors 1 (1) (2010) 6–30.
[4] T. Guo, F. Liu, B.-O. Guan, J. Albert, Tilted fiber grating mechanical and biochemical sensors, Opt. Laser Technol. 78 (2016) 19–33.
[5] L.-Y. Shao, L. Xiong, C. Chen, A. Laronche, J. Albert, Directional bend sensor based on re-grown tilted fiber Bragg grating, J. Lightwave Technol. 28 (18) (2010) 2681–2687.
[6] S. Yuezhen, Y. Zhijun, Z. Kaiming, L. Binbin, J. Biqiang, M. Chengbo, S. Qizhen, Z. Lin, Excessively tilted fiber grating sensors, J. Lightwave Technol. 39 (12) (2021) 3761–3770.
[7] R. Suo, X. Chen, K. Zhou, L. Zhang, I. Bennion, In-fibre directional transverse loading sensor based on excessively tilted fibre Bragg gratings, Meas. Sci. Technol. 20 (3) (2009) 034015.
[8] J. He, Z. Chen, X. Xu, J. He, B. Xu, B. Du, K. Guo, R. Chen, Y. Wang, Femtosecond laser line-by-line inscription of apodized fiber Bragg gratings, Opt. Lett. 46 (22) (2021) 5663.
[9] Z. Yan, Q. Sun, C. Wang, Z. Sun, C. Mou, K. Zhou, D. Liu, L. Zhang, Refractive index and temperature sensitivity characterization of excessively tilted fiber grating, Opt. Express 25 (4) (2017) 3336–3346.
[10] F. Chen, L. Binbin, D. Wu, X. Zou, L. Huang, M. Huang, Z. Liu, Two-dimensional vector bending sensor based on single excessively tilted fiber grating, Opt. Express 32 (21) (2024) 37869–37882.
[11] C. Mou, K. Zhou, Z. Yan, H. Fu, L. Zhang, Liquid level sensor based on an excessively tilted fibre grating, Opt. Commun. 305 (2013) 271–275.
[12] F. Yu, P. Xue, J. Zheng, Enhancement of refractive index sensitivity by bending a core-offset in-line fiber Mach–Zehnder interferometer, IEEE Sensors J. 19 (9) (2019) 3328–3334.
[13] H. Zhang, Z. Wu, P.P. Shum, R. Wang, X.Q. Dinh, S. Fu, W. Tong, M. Tang, Fiber Bragg gratings in heterogeneous multicore fiber for directional bending sensing, J. Opt. 18 (8) (2016) 085705.
[14] Q. Zhou, W. Zhang, L. Chen, Z. Bai, L. Zhang, L. Wang, B. Wang, T. Yan, Bending vector sensor based on a sector-shaped long-period grating, IEEE Photonics Technol. Lett. 27 (7) (2015) 713–716.
[15] W. Horsthuis, J. Fluitman, The development of fibre optic microbend sensors, Sensors Actuators 3 (1982) 99–110.
[16] K. Zhou, L. Zhang, X. Chen, I. Bennion, Optic sensors of high refractive-index responsivity and low thermal cross sensitivity that use fiber Bragg gratings of > 80° tilted structures, Opt. Lett. 31 (9) (2006) 1193–1195.
[17] J. Thomas, N. Jovanovic, R.G. Becker, G.D. Marshall, M.J. Withford, A. Tünnermann, S. Nolte, M.J. Steel, Cladding mode coupling in highly localized fiber Bragg gratings: Modal properties and transmission spectra, Opt. Express 19 (1) (2010) 325–336.
[18] J.U. Thomas, N. Jovanovic, R.G. Krämer, G.D. Marshall, M.J. Withford, A. Tünnermann, S. Nolte, M.J. Steel, Cladding mode coupling in highly localized fiber Bragg gratings II: Complete vectorial analysis, Opt. Express 20 (19) (2012) 21434–21449.
[19] T. Erdogan, Fiber grating spectra, J. Lightwave Technol. 15 (8) (1997) 1277–1294.
[20] Z. Yan, H. Wang, C. Wang, Z. Sun, G. Yin, K. Zhou, Y. Wang, W. Zhao, L. Zhang, Theoretical and experimental analysis of excessively tilted fiber gratings, Opt. Express 24 (11) (2016) 12107.
[21] J. Zhao, Y. Zhao, Y. Peng, R.-q. Lv, Q. Zhao, Review of femtosecond laser direct writing fiber-optic structures based on refractive index modification and their applications, Opt. Laser Technol. 146 (2022) 107473.
[22] A. Wolf, A. Dostovalov, K. Bronnikov, M. Skvortsov, S. Wabnitz, S. Babin, Advances in femtosecond laser direct writing of fiber Bragg gratings in multicore fibers: Technology, sensor and laser applications, Opto-Electronic Adv. 5 (4) (2022) 210055.
[23] M. Hou, K. Yang, J. He, X. Xu, S. Ju, K. Guo, Y. Wang, Two-dimensional vector bending sensor based on seven-core fiber Bragg gratings, Opt. Express 26 (18) (2018) 23770.
[24] B. Xu, J. He, X. Xu, C. Liao, X. Weng, L. Liu, J. Qu, Y. Wang, Orthogonal single-mode helical Bragg gratings created in fiber cladding for vector bending measurement, Opt. Lett. 48 (2) (2023) 452.
[25] F. Chen, X. Li, W. Bao, R. Wang, X. Qiao, Vector bending sensor based on an edge-core cladding-type fiber Bragg grating, Opt. Express 29 (23) (2021) 38720.